RSC Advances

PAPER

View Article Online
View Journal | View Issue

Cite this: *RSC Adv.*, 2021, **11**, 13876

Utilization of SAPO-18 or SAPO-35 in the bifunctional catalyst for the direct conversion of syngas to light olefins

Yuxuan Huang, Hongfang Ma, Zhiqiang Xu, Weixin Qian, Haitao Zhang and Weiyong Ying *

SAPO-18 and SAPO-35 were synthesized and utilized as the zeotype in the bifunctional catalyst for the STO process, respectively. SEM and Ar physisorption proved that SAPO-18 displayed abundant outer cages, and facilitated the diffusion of the reactant and products. NH_3-TPD revealed the adequate acid strength of SAPO-18, thus $ZnCrO_x$ + SAPO-18 bifunctional catalyst showed high selectivity to light olefins during the whole stage of the STO process. 19.9% CO conversion and 68.6% light olefins selectivity (free of CO_2) was achieved over $ZnCrO_x$ + SAPO-18(0.048) at 653 K, 1.0 MPa, GHSV = 6000 mL g^{-1} h^{-1}. The catalytic performance was stable after 6000 minutes of reaction because of the good diffusibility of SAPO-18. GC-MS and TG demonstrated that the $ZnCrO_x$ + SAPO-35 bifunctional catalyst deactivated very quickly because of the severe formation of the heavy coke deposits, which should be attributed to the acidic properties of SAPO-35 and the poor diffusibility originating from its 2-dimensional channel system. Although the $ZnCrO_x$ + SAPO-35 bifunctional catalyst exhibited high CO conversion and light olefins selectivity at the early stage of the STO process as well, its catalytic performance was unsustainable.

Received 16th March 2021
Accepted 7th April 2021

DOI: 10.1039/d1ra02087k

rsc.li/rsc-advances

Introduction

Light olefins (C_{2-4} olefins) are basic chemicals in the chemical industry, which are mainly obtained from naphtha cracking, gas cracking and fluid catalytic cracking.[1] Syngas, consisting of CO and H_2, is an important platform in C1 chemistry since it can be derived from coal, natural gas and biomass, making it a more sustainable feedstock than crude oil.[2] Thus, the direct conversion of syngas to light olefins (STO) has been investigated for decades, known as Fischer–Tropsch synthesis (FTS). However, the selectivity to light olefins among the hydrocarbon product of FTS is limited according to the Anderson–Schulz–Flory distribution model.[3–5]

Direct conversion of syngas to hydrocarbons *via* the reaction coupling strategy has received intensive attraction in recent years. The hydrocarbon distribution can be adjusted by changing the zeolite/zeotype in the bifunctional catalyst. The $ZnCrO_x$ + SAPO-34 bifunctional catalyst and ZnO–ZrO_2 + SAPO-34 bifunctional catalyst were firstly reported to be effective for the STO process in 2016.[6,7] CO was activated over the oxide surface with oxygen vacancy, forming the intermediate, which should be methanol/dimethyl ether according to the further research studies.[8,9] The intermediate was transferred to SAPO-34 *via* the gas phase, and the C–C coupling occurred inside SAPO-34 cages with acid sites. Although different metal oxides were tested for the CO activation, SAPO-34 was the most popular zeotype used in the bifunctional catalyst for the STO process.[6,7,9–13] The diffusion restriction which originated from the eight-ring pore opening of SAPO-34 led to the high selectivity to C_{2-4} hydrocarbons among the product, while the mild acid strength resulted in the high olefin/paraffin ratio (o/p).[14] When ZSM-5 acted as the zeolite in the bifunctional catalyst, the product of syngas conversion would contain a major fraction of aromatics, which should be owed to the ten-ring structure of ZSM-5.[5,15,16]

SAPO-18 is the silicoaluminophosphate with the AEI framework structure. The cages of SAPO-18 and SAPO-34 are similar to each other, but the orientation of the double six-ring unit in SAPO-18 and SAPO-34 is different.[17] SAPO-18 shows the weaker acid strength comparing with SAPO-34, and exhibits high conversion and selectivity in the methanol-to-olefins (MTO) reaction.[17–19] Since the STO reaction *via* the methanol/dimethyl ether intermediate can be understood as the combination of the methanol synthesis reaction and the MTO reaction,[9] SAPO-18 has the potential to be used as the zeotype in the bifunctional catalyst for the STO reaction. The bifunctional catalyst containing AlPO-18 or low-Si AlPO-18 displayed the satisfying catalytic performance in the STO reaction.[20] However, the bifunctional catalyst containing high content SAPO-18 has not been investigated.

SAPO-35 is the silicoaluminophosphate with the structure of levyne (LEV).[21,22] The cages in SAPO-35 are accessible through eight-ring windows, which is similar to SAPO-18. SAPO-35 has

Engineering Research Center of Large Scale Reactor Engineering and Technology, Ministry of Education, State Key Laboratory of Chemical Engineering, School of Chemical Engineering, East China University of Science and Technology, Shanghai 200237, China. E-mail: wying@ecust.edu.cn; Fax: +86 21 64252192; Tel: +86 21 64252151

been considered as a potential MTO catalyst and received some attentions in recent years.[23–25] Meanwhile, SAPO-35 deactivates faster than SAPO-18 during the MTO process. A recent research pointed out that the co-feeding H_2 during the MTO reaction could effectively prolong the catalytic lifetime of the MTO catalyst.[8] Since syngas consists of H_2 and CO, it is interesting to discuss the behaviour of the bifunctional catalyst containing SAPO-35 during the STO process under the H_2-rich atmosphere.

Herein, the bifunctional catalysts for the STO process containing SAPO-18 or SAPO-35 were prepared. $ZnCrO_x$ was the metal oxide, while SAPO-18 and SAPO-35 with different Si content were tested. XRD, ICP-OES, SEM and Ar physisorption were used to characterize the structure of the sample. The acidic properties were investigated by NH_3-TPD, and the carbonaceous species retained in the spent bifunctional catalysts after the STO reactions were analyzed by TG and GC-MS.

Experimental

Synthesis of $ZnCrO_x$

$ZnCrO_x$ was prepared by the co-precipitation method, which followed the same procedure in our previous work.[26] $Zn(NO_3)\cdot 6H_2O$ and $Cr(NO_3)\cdot 9H_2O$ were dissolved in the deionized water, and the concentration of Zn^{2+} and Cr^{3+} were both 0.5 mol L^{-1}. Ammonium carbonate was used as the precipitant. $(NH_4)_2CO_3$ aqueous solution was heated to 343 K and the nitrate solution was added dropwise under the same temperature until the pH value of the suspension reached 7.0. After aging for 3 h under 343 K, the suspension was filtrated and washed for 7 times, followed by drying at 383 K overnight. At last, the calcination was proceeded at 773 K for 1 h under the static air, and $ZnCrO_x$ was obtained.

Synthesis of SAPO-18

SAPO-18 was prepared by the hydrothermal synthesis.[27,28] Fumed silica, aluminium isopropoxide and 85% H_3PO_4 were used as the source of Si, Al and P, while the template was 35% tetraethylammonium hydroxide (TEAOH) aqueous solution. The gel composition was $SiO_2 : Al_2O_3 : H_3PO_4 : TEAOH : H_2O = a : 1 : 8 : 8 : 147$, where a varied with the different Si content. Fumed silica was added to the 35% TEAOH aqueous solution, followed by the addition of the deionized water. Subsequently, aluminium isopropoxide was added to the suspension under the agitation. After stirring for 1 h, 85% H_3PO_4 was added. Orthophosphoric acid should be added slowly (about 0.3 g min^{-1}) to prevent the aggregation, and another one-hour agitation was proceeded. The gel was placed in the PTFE-lined stainless-steel autoclave, and the autoclave was kept at 433 K for 12 h under 100 rpm rotation. The result suspension was washed by centrifuging with deionized water until the supernatant was neutral. After being dried at 383 K overnight, the sample was calcined at 873 K for 4 h with 300 mL min^{-1} air. The obtained sample was denoted as SAPO-18(x), where x represented the molar ratio of Si/(Si + Al + P) according to the ICP-OES result.

Synthesis of SAPO-35

SAPO-35 was prepared by the hydrothermal synthesis.[24] 30% silica sol, $Al(OH)_3\cdot xH_2O$ (53.57% Al_2O_3) and 85% H_3PO_4 were used as the source of Si, Al and P, while the template was hexamethyleneimine (HMI). The gel composition was $SiO_2 : Al_2O_3 : H_3PO_4 : HMI : H_2O = b : 2 : 4 : 3 : 110$, where b varied with the different Si content. $Al(OH)_3\cdot xH_2O$ was dispersed in the deionized water. 85% H_3PO_4 was added dropwise, followed by the two-hour agitation. Subsequently, 30% silica sol was added dropwise. After stirring for 1 h, HMI was added and the mixture was aged for 1 h. The gel was placed in the PTFE-lined stainless-steel autoclave, and the autoclave was kept at 473 K for 24 h under 100 rpm rotation. The result suspension was washed by centrifuging with deionized water until the supernatant was neutral. After being dried at 383 K overnight, the sample was calcined at 873 K for 6 h with 300 mL min^{-1} air. The obtained sample was denoted as SAPO-35(y), where y represented the molar ratio of Si/(Si + Al + P) according to the ICP-OES result.

Catalyst characterization

D/MAX 2550 VB/PC diffractometer was used to carry out the X-ray powder diffraction (XRD) tests. Cu Kα radiation (40 kV and 100 mA) was the X-ray source.

Agilent 725 ICP-OES instrument was used to perform the inductively coupled plasma optical emission spectrometer (ICP-OES) test. The zeotype were dissolved by hydrofluoric acid.

FEI Inspect F50 scanning electron microscope with 10 kV accelerating voltage was used to proceed the scanning electron microscopy (SEM) measurements.

Argon physisorption was carried out on the Micromeritics ASAP 2020 surface area and porosity analyzer. Before the adsorption test, the sample was degassed at 573 K for 10 hours. Argon physisorption was proceeded in liquid argon bath and the liquid argon level was held by a polymer coating. The total surface area was calculated by the BET equation. The micropore area and the external surface area were determined by the t-plot method.

Ammonia temperature programmed desorption (NH_3-TPD) tests were proceeded on the Micromeritics AutoChem II 2920 chemisorption analyzer. 0.1 g sample was pretreated at 873 K for 1 h under the flowing He. After cooling down to 333 K (or 473 K) and keeping for 30 minutes, the adsorption of ammonia was proceeded in the flowing 10% NH_3/He for 30 minutes at 333 K (or 473 K). The excess ammonia was purged by the flowing He for 30 minutes. Subsequently, TCD signal was recorded as the temperature rising to 873 K at the heating rate of 10 K min^{-1} in the flowing He.

Gas chromatography-mass spectrometry (GC-MS) tests were carried out by the Agilent 7890A and Agilent 5975C GC-MS instrument with the HP-5 capillary column. The spent bifunctional catalyst was dispersed in the deionized water. The zeotype was dissolved by hydrofluoric acid and the soluble carbonaceous species was extracted by dichloromethane.

Thermogravimetric analysis was proceeded on the Thermo-Fisher Thermax 400 instrument. The sample was heated from the room temperature to 1173 K with 100 mL min^{-1} air at the heating rate of 10 K min^{-1}.

Catalytic performance test

Catalytic performance tests of the bifunctional catalyst for the STO reaction were performed in the fix-bed stainless-steel

reactor with the quartz lining. $ZnCrO_x$ and zeotype (SAPO-18 or SAPO-35) with the same particle size (250–425 μm) were weighed after being dried by a far-infrared dryer. 340 mg $ZnCrO_x$ and 170 mg zeotype underwent thorough mixing before being loaded in the reactor. The catalyst was reduced under atmospheric H_2 at 583 K for 180 minutes, and the catalytic performance test was proceeded at 653 K, 1.0 MPa & GHSV = 6000 mL g^{-1} h^{-1} for 800 minutes. The H_2/CO ratio was 2, and 10% N_2 was used as the internal standard. The product underwent a cold trap (273 K) before being analyzed by an online Agilent 7890A GC equipped with HayeSep Q column, MolSieve 5A column and HP-AL/S column. No liquid was collected after 800 minutes of reaction and the carbon balance was higher than 98%.

CO conversion was determined by the following equation.[26]

$$X_{CO} = \frac{N_{CO,in} - N_{CO,out}}{N_{CO,in}} \times 100\% \quad (1)$$

where $N_{CO,in}$ and $N_{CO,out}$ represented the molar flow of CO at the inlet and outlet, respectively.

CO_2 selectivity was determined by the following equation.

$$S_{CO_2} = \frac{N_{CO_2,out}}{N_{CO,in} - N_{CO,out}} \times 100\% \quad (2)$$

where $N_{CO_2,out}$ represented the molar flow of CO_2 at the outlet.

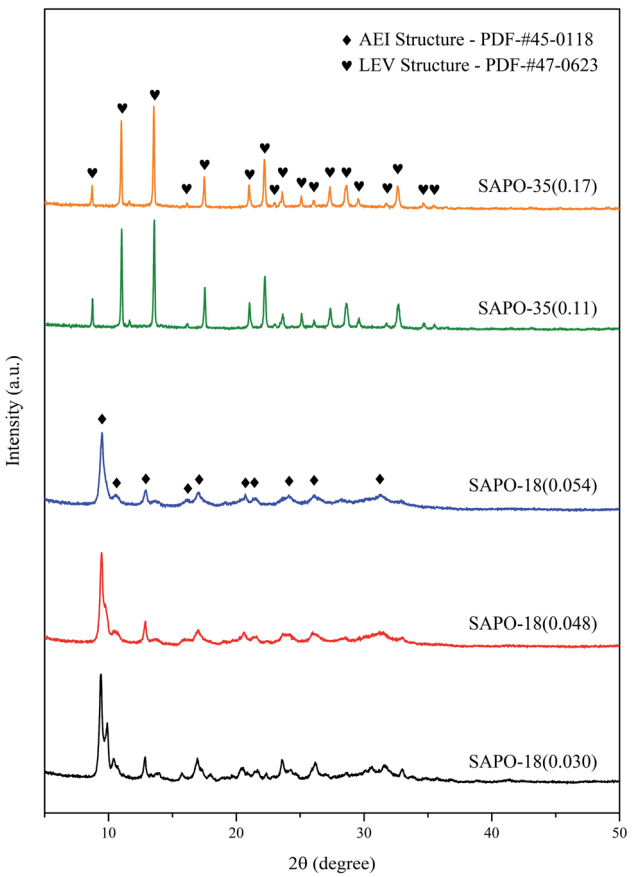

Fig. 1 XRD patterns of SAPO-18 and SAPO-35.

Table 1 Textural properties of SAPO-18 and SAPO-35

Sample	S_{BET} (m^2 g^{-1})	S_{mic} (m^2 g^{-1})	S_{ext} (m^2 g^{-1})	S_{ext}/S_{BET}
SAPO-18(0.030)	500	410	90	18%
SAPO-18(0.048)	499	391	108	22%
SAPO-18(0.054)	496	350	146	29%
SAPO-35(0.11)	399	371	28	7%
SAPO-35(0.17)	387	338	49	13%

The hydrocarbon distribution of the individual hydrocarbon C_iH_j was determined by the following equation.

$$S_{C_iH_j} = \frac{iN_{C_iH_j,out}}{\sum_1^n iN_{C_iH_j,out}} \times 100\% \quad (3)$$

where $N_{C_iH_j,out}$ represented the molar flow of C_iH_j at the outlet.

Results and discussion

Structure and acidic property

Fig. 1 displayed the XRD patterns of SAPO-18 and SAPO-35. All SAPO-18 samples showed the diffraction peaks of the AEI structure. The peak of $2\theta = 10.6°$ was the major difference between the AEI structure and the CHA structure, which proved the formation of SAPO-18. The diffusion channel system of SAPO-18 was 3-dimensional. The reactant and product could diffuse to other six cages from the central cage through the 8-ring windows and further diffuse to the whole framework, thus even if the individual 8-ring window was blocked, the whole channel system would still remain its function. SAPO-35 with different Si content showed the diffraction peaks of the LEV structure, which meant the successful synthesis of SAPO-35.[29] The diffusion channel system of SAPO-35 was 2-dimensional. The reactant and product could only diffuse to other three cages located in the same plane from the central cage through the 8-ring windows, which made the channel system is more likely to be blocked during the reaction.

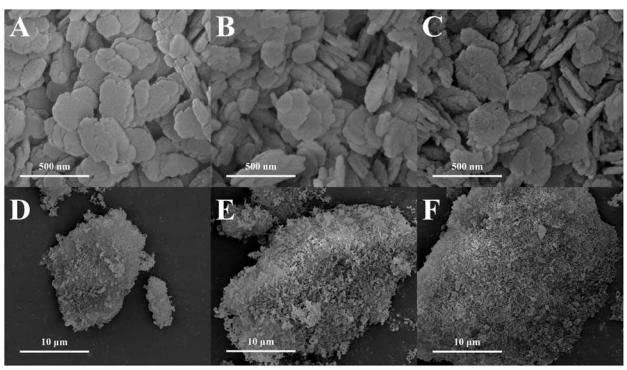

Fig. 2 SEM pictures of SAPO-18. (A) SAPO-18(0.030), 200 000×; (B) SAPO-18(0.048), 200 000×; (C) SAPO-18(0.054), 200 000×; (D) SAPO-18(0.030), 10 000×; (E) SAPO-18(0.048), 10 000×; (F) SAPO-18(0.054), 10 000×.

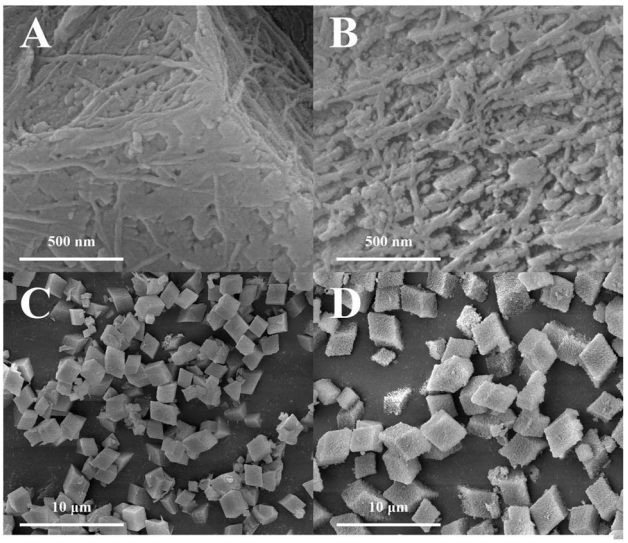

Fig. 3 SEM pictures of SAPO-35. (A) SAPO-35(0.11), 200 000×; (B) SAPO-35(0.17), 200 000×; (C) SAPO-35(0.11), 10 000×; (D) SAPO-35(0.17), 10 000×.

Table 1 showed the total surface area remained stable among SAPO-18 with different Si content, while the external surface area and its proportion kept growing as the increase of Si content, which should facilitate the diffusion of the reactant and product. However, the micropore surface became smaller at the same time. SAPO-35 showed the lower external surface area and its proportion than SAPO-18, which indicated the weaker diffusion ability of the reactant and product.

Fig. 2A–C revealed that all the SAPO-18 samples were composed of the sheet-like particles. The diameter of the particles was 200–300 nm, while the thickness was around 30 nm. Although the nanosized particles would be gathered to the micrometer-scale aggregation (Fig. 2D–F), the nanosized particles were stacked loosely, which could hardly inhibit the diffusion of the reactant and product. In addition, the cracks over the surface of the nanosized particles were more obvious as the Si content increasing in SAPO-18, which was in accord with the increasing external surface area detected by Ar physisorption. As shown in Fig. 3, SAPO-35 was composed of the micrometer-scale particles. The surface of the particle was rough, which could explain its high external surface area proportion (7–13%) comparing with other micrometer-scale zeotype particles with the similar morphology (4–5%).[26]

NH_3-TPD was used to investigate the acidic properties of the zeotype. Fig. 4A indicated that all the zeotype samples showed two ammonia desorption peaks, which corresponded to the weak acid sites and the strong acid sites, respectively.[30] Since the catalytic performance of the zeotype mainly related with the strong acid sites, the influence of the weakly held ammonia was eliminated by carrying out the ammonia adsorption at 473 K. Fig. 4B elucidated that the desorption peaks corresponding to the strong acid sites in SAPO-18 were located among 560–573 K, suggesting that the strong acid strength of SAPO-18 was mild. The desorption peaks corresponding to the strong acid sites in SAPO-35 were located around 623 K, revealing that the acid strength of SAPO-35 was stronger than SAPO-18. As shown in Table 2, the strong acid amount of SAPO-18(0.048) is higher than SAPO-18(0.030), which should be obliged to the higher Si content. However, the strong acid amount decreased in SAPO-18(0.054),

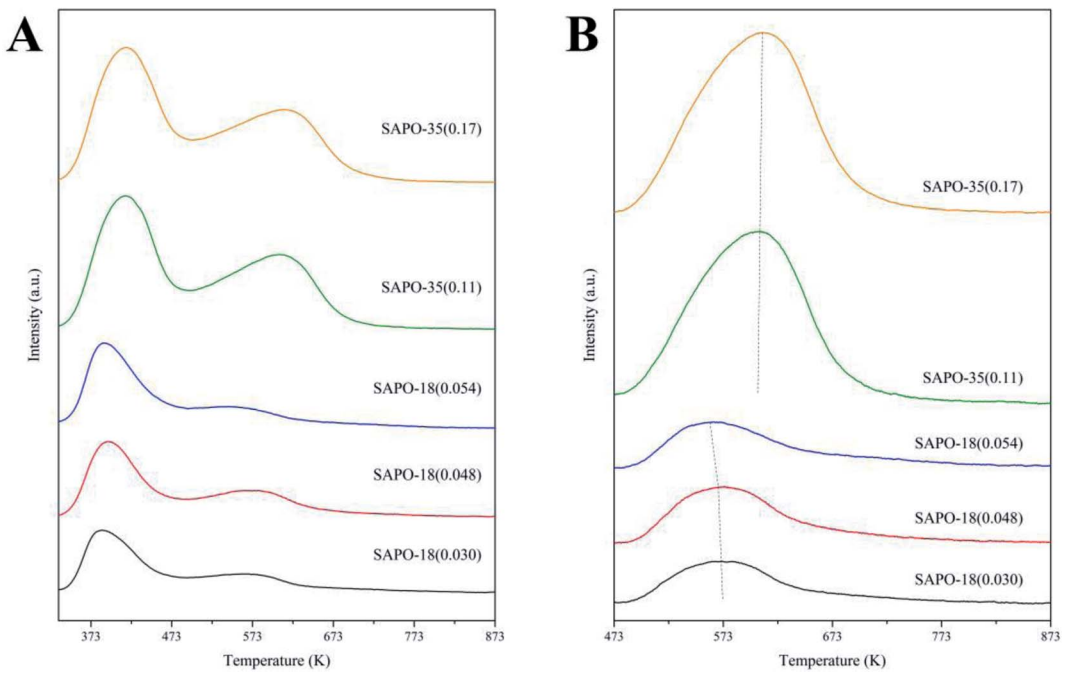

Fig. 4 NH_3-TPD profiles of SAPO-18 and SAPO-35. (A) NH_3 adsorption at 333 K; (B) NH_3 adsorption at 473 K.

Table 2 Strong acid amount of SAPO-18 and SAPO-35[a]

Sample	Strong acid amount (10^{-6} mol g^{-1})
SAPO-18(0.030)	214
SAPO-18(0.048)	278
SAPO-18(0.054)	249
SAPO-35(0.11)	850
SAPO-35(0.17)	885

[a] The calculation was based on the desorption peaks in Fig. 4B.

which should be related to the decrease of its micropore surface. Since the acid sites of SAPO-18 located in the micropore, the drop of the micropore surface would impair the existence of the acid sites. SAPO-35 displayed the higher strong acid amount than SAPO-18.

Carbonaceous species and its distribution

Methyl-benzenes and methyl-naphthalenes were generally considered as the active intermediate during the MTO process.[31] Since the STO process could be understood as the combination of the methanol synthesis reaction and the MTO reaction with H_2 co-feeding, the carbonaceous species retained in the spent bifunctional catalyst for the STO process should be similar to the intermediates formed in the zeolite/zeotype cages during the MTO process. Trimethyl-benzenes and the heavier benzenes, along with naphthalenes, were the main carbonaceous species retained in the spent bifunctional catalyst for the STO process according to our previous work.[26] As shown in Fig. 5, the carbonaceous species retained in the spent $ZnCrO_x$ + SAPO-35 bifunctional catalyst after 800 minutes of reaction were mainly dimethyl-benzenes and methyl-benzene, while little trimethyl-benzenes existed. The generally accepted intermediates for the MTO process were almost exhausted. Meanwhile, the carbonaceous species retained in the spent $ZnCrO_x$ + SAPO-18 bifunctional catalyst were mainly tetramethyl-benzenes, trimethyl-benzenes and pentamethyl-benzenes, which were highly active intermediates during the MTO process.[31]

Fig. 6A manifested that the total carbonaceous species retained in the spent $ZnCrO_x$ + SAPO-35 bifunctional catalyst was higher than those retained in the spent $ZnCrO_x$ + SAPO-18 bifunctional catalyst. Fig. 6B revealed that the carbonaceous species retained in the spent $ZnCrO_x$ + SAPO-35 bifunctional catalyst were mainly heavy coke deposits, which related with the deactivation and hard to be extracted by CH_2Cl_2, thus very little soluble carbonaceous species was detected by GC-MS. The coke formation over $ZnCrO_x$ + SAPO-35 bifunctional catalyst was more severe than $ZnCrO_x$ + SAPO-18 bifunctional catalyst during the STO process, which should be owing to the stronger acidity strength, the higher acid amount and the weaker diffusion ability of SAPO-35. The strong acidity strength and the high acid amount provided plenty of sites for carbonaceous species formation, while the diffusion of reactant and product was restricted, subsequently led to the severe formation of insoluble coke.

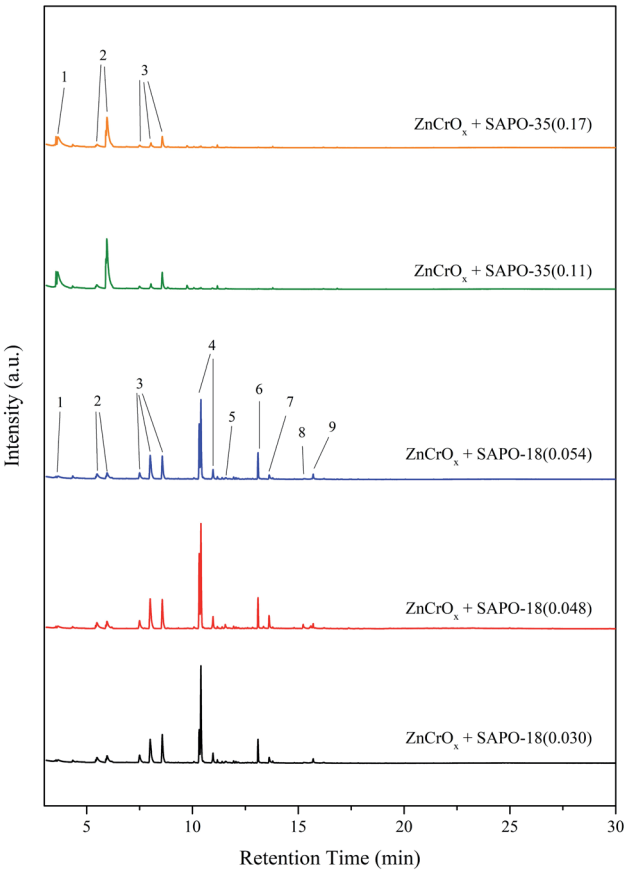

Fig. 5 Soluble carbonaceous species retained in the spent bifunctional catalyst. 1-Toluene; 2-xylenes; 3-trimethyl-benzenes; 4-tetramethyl-benzenes; 5-naphthalenes; 6-pentamethyl-benzenes; 7-methyl-naphthalenes; 8-dimethyl-naphthalenes; 9-hexamethyl-benzenes.

Catalytic performance and the structure–performance relationship

As shown in Table 3, all the bifunctional catalysts containing SAPO-18 or SAPO-35 displayed high CO conversion and high selectivity to light olefins (free of CO_2) at the early stage (TOS = 20 min) of the STO process. 19.9% CO conversion and 68.6% light olefins selectivity (free of CO_2) was achieved over $ZnCrO_x$ + SAPO-18(0.048) bifunctional catalyst at 653 K, 1.0 MPa, GHSV = 6000 mL g^{-1} h^{-1}. As the reaction progress, CO conversion decreased to 14.1% and light olefins selectivity (free of CO_2) raised to 84.4% after 800 minutes of reaction. The catalytic performance was stable within 6000 minutes of reaction (Fig. 7). As shown in Table 4, $ZnCrO_x$ + SAPO-18(0.048) bifunctional catalyst showed the highest CO conversion among all the $ZnCrO_x$ + SAPO-18 bifunctional catalyst at the stable period (TOS = 800 min) of the reaction, which should be owed to the adequate textural property and strong acid amount of SAPO-18(0.048). Comparing with SAPO-18(0.030), SAPO-18(0.048) displayed higher strong acid amount and the higher proportion of the external surface, exposing more outer cages and facilitating the diffusion of the reactant and product, which was beneficial to maintain

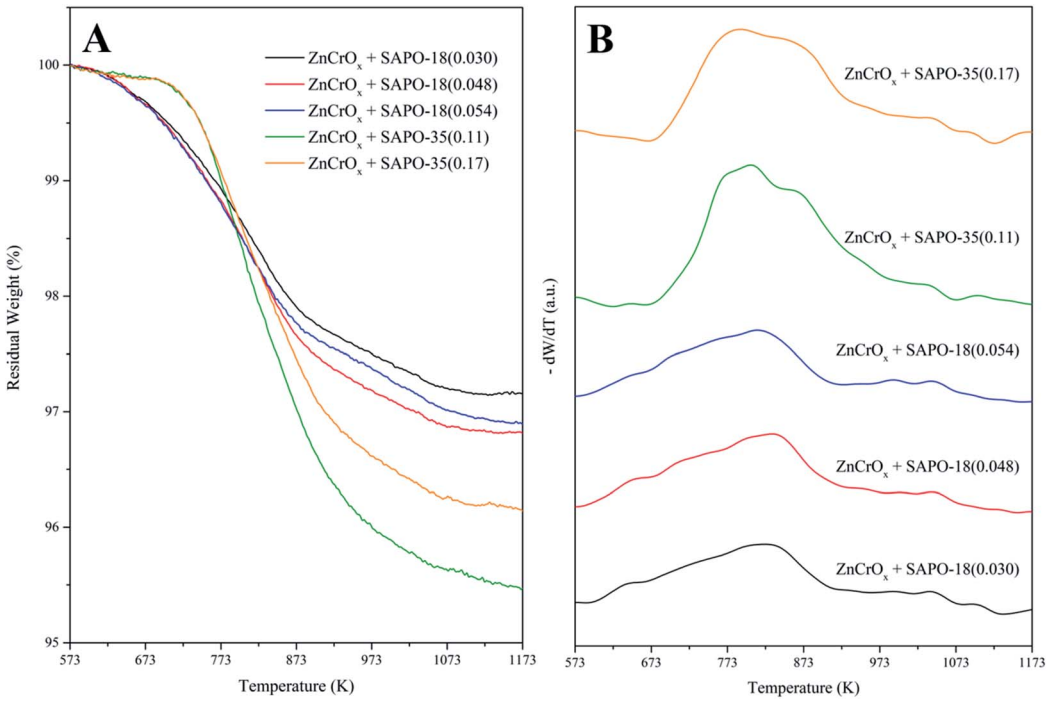

Fig. 6 TG profiles (A) and DTG profiles (B) of the spent bifunctional catalyst (TOS = 800 min).

the high activity of the bifunctional catalyst during the STO process. However, the proportion of the external surface in SAPO-18(0.054) was too high, which corresponded to the reduced micropore surface and strong acid amount, resulting in the decrease of activity. This deduction was in good consistence with the slightly decreased desorption peak area and desorption peak temperature of SAPO-18(0.054) in the NH_3-TPD experiment (Fig. 4B & Table 2) comparing with SAPO-18(0.048). The defect on the surface of SAPO-18(0.054) implied that the excess proportion of the external surface slightly damaged the particle structure (Fig. 2).

The high selectivity to light olefins (free of CO_2) over $ZnCrO_x$ + SAPO-18 bifunctional catalyst at the early stage should be attributed to the appropriate acid strength of SAPO-18. The acid strength of SAPO-18 was weak, thus the hydrogen transfer reaction during the induction period was inhibited. Since the STO process *via* the oxide-zeolite strategy could be understood as the combination of the methanol synthesis reaction and the MTO reaction with H_2 co-feeding, the inhibition of the hydrogen transfer reaction at the induction period in the MTO process should be benefit to increase the light olefins selectivity (free of CO_2) at the early stage in the STO process.

$ZnCrO_x$ + SAPO-35(0.11) displayed 16.5% CO conversion and 75.1% light olefins selectivity (free of CO_2) at 653 K, 1.0 MPa, GHSV = 6000 mL g^{-1} h^{-1} and TOS = 20 min. The olefin/paraffin (o/p) ratio was 6.54. However, the activity of $ZnCrO_x$ + SAPO-35(0.11) bifunctional catalyst decreased very quickly. CO conversion dropped to 5.68%, while the selectivity to light olefins among the hydrocarbon products decreased to 57.1% after only 100 minutes of reaction. As the reaction progress, the deactivation became deeper, which made the discussion based on the catalytic performance over

Table 3 Catalytic performance of the STO reaction over the bifunctional catalyst (TOS = 20 min)[a]

Zeotype in bifunctional catalyst	CO conversion (%)	Hydrocarbon distribution (%)				CO_2 selectivity (%)	C_{2-4} o/p
		CH_4	C2–4$^=$	C2–4^0	C_{5+}		
SAPO-18(0.030)	17.2	1.6	75.1	11.6	11.8	49.9	6.5
SAPO-18(0.048)	19.9	2.3	68.6	16.2	12.9	49.2	4.2
SAPO-18(0.054)	18.2	1.8	69.9	13.0	15.4	49.4	5.4
SAPO-35(0.11)	16.5	9.7	75.1	11.5	3.7	47.4	6.5
SAPO-35(0.17)	13.9	7.1	74.2	17.7	1.0	46.9	4.2

[a] Reduction condition: 583 K, atmospheric H_2, GHSV = 6000 mL g^{-1} h^{-1}. Reaction condition: 653 K, 1.0 MPa, GHSV = 6000 mL g^{-1} h^{-1}, TOS = 20 min, $H_2/CO/N_2$ = 6/3/1, OX/ZEO = 2.

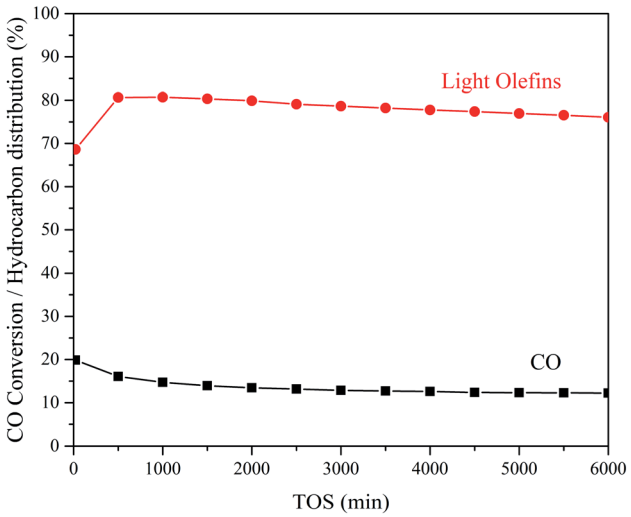

Fig. 7 Stability test of the catalytic performance for the STO reaction over $ZnCrO_x$ + SAPO-18(0.048) bifunctional catalyst. Reduction condition: 583 K, atmospheric H_2, GHSV = 6000 mL g^{-1} h^{-1}. Reaction condition: 653 K, 1.0 MPa, GHSV = 6000 mL g^{-1} h^{-1}, TOS = 6000 min, $H_2/CO/N_2$ = 6/3/1, OX/ZEO = 2.

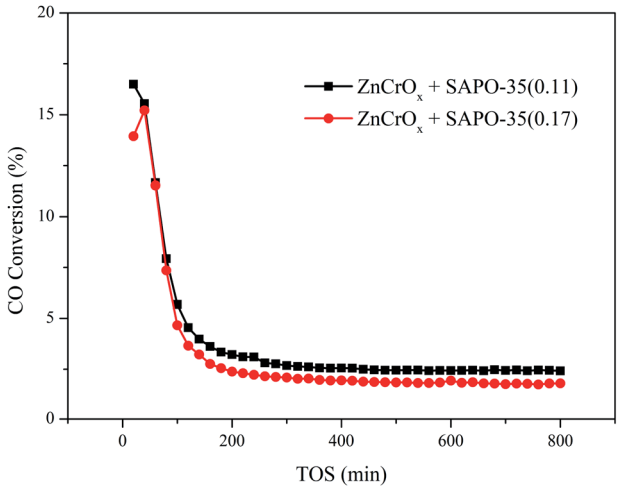

Fig. 8 CO conversion along with the reaction progress over $ZnCrO_x$ + SAPO-35 bifunctional catalyst.

$ZnCrO_x$ + SAPO-35 bifunctional catalyst at TOS = 800 min meaningless (Fig. 8).

The lifetime of $ZnCrO_x$ + SAPO-35 bifunctional catalyst was short, thus the induction period was condensed and the stable period came earlier, resulting in the high selectivity to light olefins at TOS = 20 min. However, this kind of high selectivity to light olefins was unsustainable. Since the aromatics were the essential intermediate during the MTO process,[9,32] while benzenes and naphthalenes had the potential to develop into the polyclinic aromatics, the 2-dimensional channel system of SAPO-35 would be blocked easily. The MTO reaction which occurred in the zeotype consumed methanol, provided the thermodynamic driving force to the CO activation over the metal oxide and led to the high CO conversion during the STO process. The block of the zeotype would impair the methanol consumption, and weaken the thermodynamic driving force, resulting in the lower CO conversion during the STO process. Although the H_2-rich atmosphere could slow down the evolution of coke species and prolong the catalytic lifetime,[8] the bifunctional catalyst containing SAPO-35 still showed the short lifetime. The block of the channel system would facilitate the formation of the larger coke compounds and graphitic deposits, leading to the fast catalyst deactivation.[33] The absence of the active intermediates retained in the spent $ZnCrO_x$ + SAPO-35 bifunctional catalyst was consistent with the deactivation after 800 minutes of reaction.

The lifetime of $ZnCrO_x$ + SAPO-35 bifunctional catalyst was short because of the severe coke formation originated from the acidic strength, acid amount and 2-dimensional channel system of SAPO-35. Thus, the stable period came early, resulting in the high CO conversion and high selectivity to light olefins at the early stage of the process. However, this kind of catalytic performance was unsustainable. $ZnCrO_x$ + SAPO-35 bifunctional catalyst would deactivate very quickly.

The 3-dimensional channel system of SAPO-18 and the nanosized sheet-like morphology of SAPO-18 particles facilitated the diffusion of the reactant and products, resulting in the lower content of total carbonaceous species retained in the spent $ZnCrO_x$ + SAPO-18 bifunctional catalyst comparing with the spent $ZnCrO_x$ + SAPO-35 bifunctional catalyst (Fig. 6A), and led to the sustainable catalytic performance within 6000 minutes of reaction. Meanwhile, the acid strength of SAPO-18 was weak, resulting in the high selectivity to light olefins during the whole period of the STO process, including the induction period and the stable period.

Table 4 Catalytic performance of the STO reaction over $ZnCrO_x$ + SAPO-18 bifunctional catalyst (TOS = 800 min)[a]

Zeotype in bifunctional catalyst	CO conversion (%)	Hydrocarbon distribution (%)				CO_2 selectivity (%)	C_{2-4} o/p
		CH_4	C2–4$^{=}$	C2–4°	C_{5+}		
SAPO-18(0.030)	12.4	3.5	85.6	3.7	7.3	52.0	23.3
SAPO-18(0.048)	14.1	3.3	84.4	4.1	8.2	51.5	20.6
SAPO-18(0.054)	12.4	4.3	82.7	4.3	8.6	51.9	19.5

[a] Reduction condition: 583 K, atmospheric H_2, GHSV = 6000 mL g^{-1} h^{-1}. Reaction condition: 653 K, 1.0 MPa, GHSV = 6000 mL g^{-1} h^{-1}, TOS = 800 min, $H_2/CO/N_2$ = 6/3/1, OX/ZEO = 2.

Conclusions

The appropriate acid strength of SAPO-18 resulted in the high selectivity to light olefins during the whole period of STO process over $ZnCrO_x$ + SAPO-18 bifunctional catalyst. The 3-dimensional channel system and the nanosized sheet-like morphology of SAPO-18 facilitated the diffusion of the reactant and product, thus the carbonaceous species retained in the SAPO-18 cages were highly active methyl-benzenes, making the catalytic performance over $ZnCrO_x$ + SAPO-18 bifunctional catalyst sustainable. The strong acidic strength and acid amount of SAPO-35 facilitated the carbonaceous species formation, and the 2-dimensional channel system of SAPO-35 inhibited the diffusion, thus mass heavy coke deposits generated, and severely shortened the lifetime of $ZnCrO_x$ + SAPO-35 bifunctional catalyst. As the consequence, the stable period of the STO process came early, displaying high CO conversion and high selectivity to light olefins. However, this was an unsustainable catalytic performance as $ZnCrO_x$ + SAPO-35 bifunctional catalyst deactivated very quickly. $ZnCrO_x$ + SAPO-18 bifunctional catalyst and $ZnCrO_x$ + SAPO-35 bifunctional catalyst both displayed high CO conversion and high selectivity to light olefins at the early stage of the STO process. 19.9% CO conversion and 68.6% light olefins selectivity (free of CO_2) was achieved over $ZnCrO_x$ + SAPO-18(0.048). CO conversion was stable after 6000 minutes of reaction and the selectivity to light olefins was high throughout the whole period during the STO process.

Conflicts of interest

There are no conflicts to declare.

Acknowledgements

This work is supported by National High Technology Reserch and Development Plan of China (863 plan, No. 2011AA05A204).

Notes and references

1 H. M. Torres Galvis and K. P. de Jong, Catalysts for Production of Lower Olefins from Synthesis Gas: A Review, *ACS Catal.*, 2013, **3**, 2130–2149.
2 J. Goetze, Operando Spectroscopy on the Reaction Mechanism and Deactivation of Methanol-to-Olefins Catalysts, PhD thesis, Utrecht University, 2018.
3 L. Zhong, F. Yu, Y. An, Y. Zhao, Y. Sun, Z. Li, T. Lin, Y. Lin, X. Qi, Y. Dai, L. Gu, J. Hu, S. Jin, Q. Shen and H. Wang, Cobalt Carbide Nanoprisms for Direct Production of Lower Olefins from Syngas, *Nature*, 2016, **538**, 84–87.
4 Y. Cheng, J. Lin, K. Xu, H. Wang, X. Yao, Y. Pei, S. Yan, M. Qiao and B. Zong, Fischer–Tropsch Synthesis to Lower Olefins over Potassium-Promoted Reduced Graphene Oxide Supported Iron Catalysts, *ACS Catal.*, 2016, **6**, 389–399.
5 W. Zhou, K. Cheng, J. Kang, C. Zhou, V. Subramanian, Q. Zhang and Y. Wang, New Horizon in C1 Chemistry: Breaking the Selectivity Limitation in Transformation of Syngas and Hydrogenation of CO2 into Hydrocarbon Chemicals and Fuels, *Chem. Soc. Rev.*, 2019, **48**, 3193–3228.
6 K. Cheng, B. Gu, X. Liu, J. Kang, Q. Zhang and Y. Wang, Direct and Highly Selective Conversion of Synthesis Gas into Lower Olefins: Design of a Bifunctional Catalyst Combining Methanol Synthesis and Carbon–Carbon Coupling, *Angew. Chem., Int. Ed.*, 2016, **55**, 4725–4728.
7 F. Jiao, J. Li, X. Pan, J. Xiao, H. Li, H. Ma, M. Wei, Y. Pan, Z. Zhou, M. Li, S. Miao, J. Li, Y. Zhu, D. Xiao, T. He, J. Yang, F. Qi, Q. Fu and X. Bao, Selective Conversion of Syngas to Light Olefins, *Science*, 2016, **351**, 1065–1068.
8 X. Zhao, J. Li, P. Tian, L. Wang, X. Li, S. Lin, X. Guo and Z. Liu, Achieving a Superlong Lifetime in the Zeolite-Catalyzed MTO Reaction under High Pressure: Synergistic Effect of Hydrogen and Water, *ACS Catal.*, 2019, **9**, 3017–3025.
9 Y. Ni, Y. Liu, Z. Chen, M. Yang, H. Liu, Y. He, Y. Fu, W. Zhu and Z. Liu, Realizing and Recognizing Syngas-to-Olefins Reaction via a Dual-Bed Catalyst, *ACS Catal.*, 2019, **9**, 1026–1032.
10 J. Su, D. Wang, Y. Wang, H. Zhou, C. Liu, S. Liu, C. Wang, W. Yang, Z. Xie and M. He, Direct Conversion of Syngas into Light Olefins over Zirconium-Doped Indium(III) Oxide and SAPO-34 Bifunctional Catalysts: Design of Oxide Component and Construction of Reaction Network, *ChemCatChem*, 2018, **10**, 1536–1541.
11 Y. Zhu, X. Pan, F. Jiao, J. Li, J. Yang, M. Ding, Y. Han, Z. Liu and X. Bao, Role of Manganese Oxide in Syngas Conversion to Light Olefins, *ACS Catal.*, 2017, **7**, 2800–2804.
12 N. Li, F. Jiao, X. Pan, Y. Ding, J. Feng and X. Bao, Size Effects of ZnO Nanoparticles in Bifunctional Catalysts for Selective Syngas Conversion, *ACS Catal.*, 2019, **9**, 960–966.
13 G. Raveendra, C. Li, B. Liu, Y. Cheng, F. Meng and Z. Li, Synthesis of Lower Olefins from Syngas over Zn/Al2O3–SAPO-34 Hybrid Catalysts: Role of Doped Zr and Influence of the Zn/Al2O3 Ratio, *Catal. Sci. Technol.*, 2018, **8**, 3527–3538.
14 B. Hereijgers, F. Bleken, M. Nilsen, S. Svelle, K. Lillerud, M. Bjørgen, B. Weckhuysen and U. Olsbye, Product Shape Selectivity Dominates the Methanol-to-Olefins (MTO) Reaction over H-SAPO-34 Catalysts, *J. Catal.*, 2009, **264**, 77–87.
15 J. Yang, X. Pan, F. Jiao, J. Li and X. Bao, Direct Conversion of Syngas to Aromatics, *Chem. Commun.*, 2017, **53**, 11146–11149.
16 K. Cheng, W. Zhou, J. Kang, S. He, S. Shi, Q. Zhang, Y. Pan, W. Wen and Y. Wang, Bifunctional Catalysts for One-Step Conversion of Syngas into Aromatics with Excellent Selectivity and Stability, *Chem*, 2017, **3**, 334–347.
17 J. Chen, P. Wright, J. Thomas, S. Natarajan, L. Marchese, S. Bradley, G. Sankar, C. Catlow, P. Gai-Boyes, R. Townsend and C. Lok, SAPO-18 Catalysts and Their Broensted Acid Sites, *J. Phys. Chem.*, 1994, **98**, 10216–10224.
18 J. Chen, P. Wright, S. Natarajan and J. Thomas, Understanding The Brønsted Acidity of Sapo-5, Sapo-17, Sapo-18 and SAPO-34 and Their Catalytic Performance for

Methanol Conversion to Hydrocarbons, *Stud. Surf. Sci. Catal.*, 1994, **84**, 1731–1738.

19 Y. Hirota, M. Yamada, Y. Uchida, Y. Sakamoto, T. Yokoi and N. Nishiyama, Synthesis of SAPO-18 with Low Acidic Strength and Its Application in Conversion of Dimethylether to Olefins, *Microporous Mesoporous Mater.*, 2016, **232**, 65–69.

20 J. Su, H. Zhou, S. Liu, C. Wang, W. Jiao, Y. Wang, C. Liu, Y. Ye, L. Zhang, Y. Zhao, H. Liu, D. Wang, W. Yang, Z. Xie and M. He, Syngas to Light Olefins Conversion with High Olefin/paraffin Ratio Using ZnCrOx/AlPO-18 Bifunctional Catalysts, *Nat. Commun.*, 2019, **10**, 1297.

21 B. Lok, C. Messina, R. Patton, R. Gajek, T. Cannan and E. Flanigen, Silicoaluminophosphate Molecular Sieves: Another New Class of Microporous Crystalline Inorganic Solids, *J. Am. Chem. Soc.*, 1984, **106**, 6092–6093.

22 N. Venkatathri and J. Yoo, Synthesis, Characterization and Catalytic Properties of A LEV Type Silicoaluminophosphate Molecular Sieve, SAPO-35 from Aqueous Media Using Aluminium Isopropoxide and Hexamethyleneimine Template, *Appl. Catal., A*, 2008, **340**, 265–270.

23 B. Li, P. Tian, J. Li, J. Chen, Y. Yuan, X. Su, D. Fan, Y. Wei, Y. qi and Z. Liu, Synthesis of SAPO-35 Molecular Sieve and Its Catalytic Properties in the Methanol-to-olefins Reaction, *Chin. J. Catal.*, 2013, **34**, 798–807.

24 I. Pinilla-Herrero, U. Olsbye, C. Márquez-Álvarez and E. Sastre, Effect of Framework Topology of SAPO Catalysts on Selectivity and Deactivation Profile in the Methanol-to-olefins Reaction, *J. Catal.*, 2017, **352**, 191–207.

25 N. Katada, K. Nouno, J. Lee, J. Shin, S. Hong and M. Niwa, Acidic Properties of Cage-Based, Small-Pore Zeolites with Different Framework Topologies and Their Silicoaluminophosphate Analogues, *J. Phys. Chem. C*, 2011, **115**, 22505–22513.

26 Y. Huang, H. Ma, Z. Xu, W. Qian, H. Zhang and W. Ying, Role of Nanosized Sheet-like SAPO-34 in Bifunctional Catalyst for Syngas-to-Olefins Reaction, *Fuel*, 2020, **273**, 117771.

27 H. van Heyden, S. Mintova and T. Bein, Nanosized SAPO-34 Synthesized from Colloidal Solutions, *Chem. Mater.*, 2008, **20**, 2956–2963.

28 Z. Xu, J. Li, W. Qian, H. Ma, H. Zhang and W. Ying, Synthesis of Core–Shell SAPO-34@SAPO-18 Composites by the Epitaxial Growth Method and Their Catalytic Properties for the MTO Reaction, *RSC Adv.*, 2017, **7**, 54866–54875.

29 I. Pinilla-Herrero, L. Gómez-Hortigüela, C. Márquez-Álvarez and E. Sastre, Unexpected Crystal Growth Modifier Effect of Glucosamine as Additive in the Synthesis of SAPO-35, *Microporous Mesoporous Mater.*, 2016, **219**, 322–326.

30 N. Katada, H. Igi, J. Kim and M. Niwa, Determination of the Acidic Properties of Zeolite by Theoretical Analysis of Temperature-Programmed Desorption of Ammonia Based on Adsorption Equilibrium, *J. Phys. Chem. B*, 1997, **101**, 5969–5977.

31 W. Song, H. Fu and J. Haw, Selective Synthesis of Methylnaphthalenes in HSAPO-34 Cages and Their Function as Reaction Centers in Methanol-to-Olefin Catalysis, *J. Phys. Chem. B*, 2001, **105**, 12839–12843.

32 J. Haw, W. Song, D. Marcus and J. Nicholas, The Mechanism of Methanol to Hydrocarbon Catalysis, *Acc. Chem. Res.*, 2003, **36**, 317–326.

33 D. Mores, E. Stavitski, M. Kox, J. Kornatowski, U. Olsbye and B. Weckhuysen, Space- and Time-Resolved In-situ Spectroscopy on the Coke Formation in Molecular Sieves: Methanol-to-Olefin Conversion over H-ZSM-5 and H-SAPO-34, *Chem.–Eur. J.*, 2008, **14**, 11320–11327.